Millimeter-wave spectroscopy in cesium Rydberg states. Quantum defects, fine- and hyperfine-structure measurements

P. Goy, J. M. Raimond, G. Vitrant, and S. Haroche
Laboratoire de Physique de l'Ecole Normale Supérieure, 24 rue Lhomond, 75231 Paris Cedex 05, France
(Received 28 October 1981)

High-resolution double-resonance spectroscopy experiments in the millimeter-wave domain have yielded precise values of quantum defects in the S, P, D, and F Rydberg levels of cesium (principal quantum number n ranging from 23 to 45). In addition, fine and hyperfine structures have been measured in these levels. These experiments provide a precise mapping of the cesium Rydberg levels, allowing us to predict with an accuracy of about a MHz any transition frequency between two states with $n \geq 20$ and $l \leq 3$.

I. GENERAL DESCRIPTION OF EXPERIMENTS

We present here the results of an extensive double-resonance spectroscopy study of cesium Rydberg states. We have obtained new precise values of quantum defects in S, P, D and F levels as well as fine structures in P, D, and F states and hyperfine-structure intervals in the $S_{1/2}$ and $P_{1/2}$ levels, for principal quantum numbers n in the range 23 to 45. These experiments provide a precise mapping of the Rydberg states of cesium with angular momentum $l \leq 3$ and allow us to predict any transition frequency between these levels with an accuracy of about a MHz.

The set up and the spectroscopic techniques are in their principle identical to those used in earlier experiments on Na atoms.[1-3] We refer the reader to the corresponding papers for details. Let us just recall here that the atoms propagating in an atomic beam are prepared in an nS or an nD level by stepwise pulsed laser excitation. (In the case of cesium, this excitation involves an infrared laser at 8521 Å for the $6S_{1/2} \rightarrow 6P_{3/2}$ transition and a green laser around 5100 Å for the $6P_{3/2} \rightarrow nS$ or nD ones.) Millimeter-wave transitions are then induced towards nearby levels and detected by the field ionization method.[1] The only significant improvement over the previous Na experiment concerns our mm-wave sources. Our carcinotrons can now be locked to the harmonic of a stabilized X-band klystron up to 480 GHZ, as compared to 120 GHz only in Ref. 2. Furthermore, the millimeter harmonic signal of the 11–12-GHz klystron produced by a Schottky diode (the same which is used as a reference to lock the carcinotrons) is powerful enough to directly induce transitions between Rydberg levels, so that carcinotrons are in some cases no longer needed. Details about the improved carcinotrons stabilization and frequency multiplying technique are published elsewhere.[4]

II. OBSERVED TRANSITIONS

Figure 1 presents an energy diagram of cesium Rydberg levels indicating with arrows the transitions we have observed. They involve single pho-

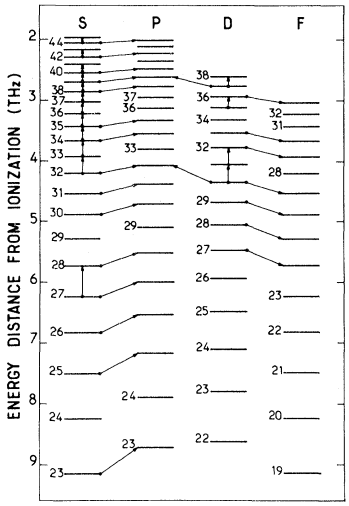

FIG. 1. Section of the cesium atom energy diagram near the ionization limit. Arrows represent the microwave transitions observed in this work (for sake of clarity, we do not distinguish the fine-structure components).

ton $nS_{1/2} \rightarrow nP_{1/2,3/2}$; $nD_{5/2} \rightarrow (n-3)F_{5/2,7/2}$; $nD_{5/2} \rightarrow nP_{3/2}$ as well as two-photon $nS_{1/2} \rightarrow (n+1)S_{1/2}$ and $nD_{5/2} \rightarrow (n+1)D_{5/2,3/2}$ transitions. For the sake of clarity, we have not represented the fine structure of the P, D, and F states in the figure; each arrow corresponds, in general, to more than one nondegenerate transition.

Owing to the extremely large size of the electric-dipole matrix elements in Rydberg levels,[1] single-photon transitions require very small microwave powers to be saturated during the ~ 5-μs interaction time with the microwave. Typically, a power flux of 10^{-10} W/cm^2 is enough; it can be delivered either by a carcinotron or by the frequency multiplied output of a Schottky diode powered by an X-band klystron (we have used up to the 28th harmonic). Two-photon transitions are favored by the occurrence of an intermediate level close to the middle of the transition gap. The coincidence is particularly good for the $nS \rightarrow (n+1)S$ resonances: the $nP_{3/2}$ level is 3.6 GHz away from the middle of the gap for $n=27$ and only 8 MHz away for $n=42$. As a result, these transitions require rather small saturating powers (10^{-4} W/cm^2 for $n=27$ and only 10^{-8} W/cm^2 for $n=42$) and most of them can also be induced by direct frequency multiplication. The $nD \rightarrow (n+1)D$ transitions on the other hand, rely on the $(n-2)F$ intermediate level, which does not coincide as well with the middle of the transition gap (16 GHz for $n=30$). Larger amounts of microwave are thus required for these transitions ($\sim 10^{-3}$ W/cm^2) and the big powers delivered by the carcinotrons are then needed.

Typical linewidths range from ~ 300 kHz for some S-S two-photon lines up to a few MHz for single-photon resonances. The main limitation to the linewidths seems to be the existence of stray electric-field inhomogeneities (~ 100 mV/cm), whereas the Doppler effect (~ 100 kHz at 120 GHz) affects only the narrowest S-S two-photon lines. (Let us note that, contrary to the Na spectroscopy experiments,[2] we have not tried to suppress the Doppler effect on two-photon line by taking advantage of the standing-wave method. All our experiments have been performed without a microwave cavity.)

The resonances involving $S_{1/2}$ and $P_{1/2}$ levels exhibit splittings due to the hyperfine interaction of the valence electron with the $I=\frac{7}{2}$ nuclear spin of Cs. Figure 2 presents a typical example of a recording of the $28S_{1/2} \rightarrow 28P_{1/2}$ resonance with an insert giving the assignment of the hyperfine components. The hyperfine splitting of the $28S_{1/2}$ state (4.7 ± 0.8 MHz) is clearly resolved, and the smaller one of the $28P_{1/2}$ level (1.1 ± 0.2 MHz) is barely observable. This hyperfine interaction is also apparent on the two-photon $nS \rightarrow (n+1)S$ lines. Figure 3 shows two recordings of the $36S_{1/2} \rightarrow 37S_{1/2}$ resonance as an example. The two $\Delta F=0$ transitions (which are the only ones allowed) have their frequencies separated by half the difference between the 36S and 37S hyperfine intervals, i.e., only ~ 70 kHz. Similar structures were not observed in our earlier Na experiments due to a much smaller hyperfine coupling in this lighter alkali. These recordings (Figs. 2 and 3) provide, to our knowledge, the first example of hyperfine-structure effects due to a very excited valence electron. The yet closer hyperfine com-

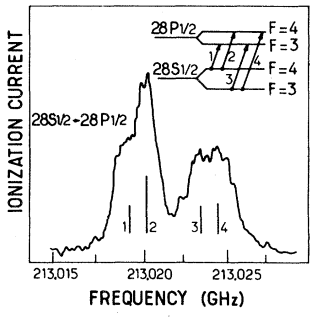

FIG. 2. Recording of the $28S_{1/2} \rightarrow 28P_{1/2}$ transition. The hyperfine components are identified by the numbered arrows in the insert.

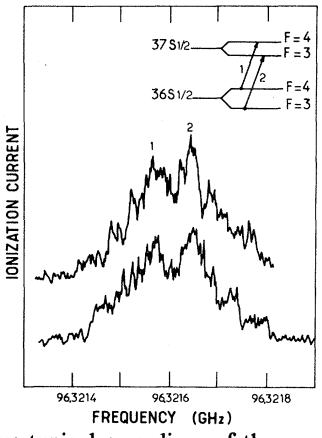

FIG. 3. Two typical recordings of the $36S_{1/2} \rightarrow 37S_{1/2}$ two-photon resonance. Frequency scale refers to the mm-wave source. Energy interval corresponds to twice this frequency. Two $\Delta F=0$ allowed hyperfine components are identified by the arrows in the insert. ~ 70-kHz apart lines are consistently resolved.

ponents of the $nP_{3/2}$, nD, and nF Rydberg levels were not consistently separated at our resolution level. Much easier to resolve are of course the fine-structure intervals. In nP levels they are very large and have been measured over a wide range of n values ($23 \leq n \leq 42$). In D states they have been very difficult to observe due to the fact that the laser excitation prepared mostly the $nD_{5/2}$ level and only very weakly the $nD_{3/2}$ level. We have been able to measure only the $32D$ fine-structure interval on the two-photon $31D_{5/2} \rightarrow 32D_{5/2,3/2}$ transitions. nF fine structures have been easier to observe. Figure 4 shows an example of the resonances corresponding to the observation of the $24F$ doublet. The fine structure in the F Rydberg levels is inverted as known from Ref. 5, which explains the ordering of states in the insert and the assignment of the two components of the spectrum.

All the frequencies measured in our set of experiments are given in Table I with the corresponding uncertainties. These uncertainties are the statistical dispersions over a large number of determinations of the line-frequency centers. They are thus roughly proportional to the linewidth of the corresponding resonance. For resonances exhibiting a hyperfine splitting, the center frequency of the whole structure is given. (The last column of this table will be discussed in Sec. III.) Table II gathers the fine-structure intervals of the P, D, F levels obtained by making the differences of the frequencies given in Table I. For sake of comparison, some fine-structure intervals of more bound states previously measured in other works

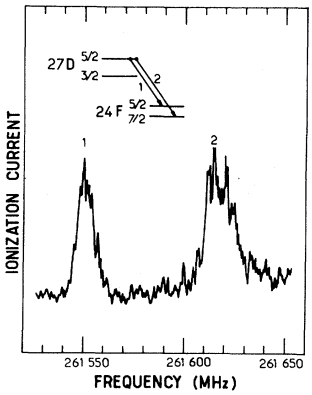

FIG. 4. Recording of the $27D_{5/2} \rightarrow 24F_{5/2}$ and $27D_{5/2} \rightarrow 24F_{7/2}$ resonances allowing us to measure the $24F$ fine-structure interval. Arrows in the insert give the line assignment (note the inverted fine structure in the F level).

are added to this table, whose last column will be explained in Sec. IV. At last, Table III gathers the data we have obtained on hyperfine-structure intervals.

III. ANALYSIS OF THE DATA: QUANTUM DEFECTS

Any frequency interval $\nu(nlJ \rightarrow n'l'J')$ between two states n,l,J and $n'l'J'$ can be expressed by the Rydberg formula involving the quantum defects of the levels

$$h\nu(nlJ \rightarrow n'l'J') = R_{Cs}\{[n - \epsilon_{lj}(n)]^{-2} - [n' - \epsilon_{l'J'}(n')]^{-2}\}, \quad (1)$$

where

$$R_{Cs} = 3.289\,828\,299(20) \times 10^9 \text{ MHz}$$

is the Rydberg constant for the reduced electron mass in cesium and $\epsilon_{lJ}(n)$ are the quantum defects of the initial and final states, which mainly depend on l and only slightly on J and n. The n dependence can be expressed by the Ritz formula

$$\epsilon_{lJ}(n) = \epsilon_{lJ}(\infty) + a_{lJ}[n - \epsilon_{lj}(\infty)]^{-2} + \cdots, \quad (2)$$

where only the first two terms are relevant for Rydberg levels with $n \gtrsim 20$. It is remarkable that all the data in Table I can be fitted by formula (1) by assigning an unique value to each ϵ_{lJ} and a_{lJ} coefficient in (2). The $\epsilon_{0,1/2}$ and $\epsilon_{2,5/2}$ values are obtained by analyzing the two-photon line $S_{1/2} \rightarrow S_{1/2}$ and $D_{5/2} \rightarrow D_{5/2}$ frequency data according to the method already described in Ref. 2. Each transition frequency yields at first an "average" quantum defect $\epsilon^*(n)$ for the couple of relevant levels. Extrapolation of $\epsilon^*(n)$ to $n = \infty$ then yields $\epsilon_l(\infty)$ ($l = 0,2$). Knowing these values, the measured frequency of each two-photon line gives in turn a value of the a_{lJ} coefficient, which is found to be the same for all the transitions. One can then calculate the $\epsilon_{0,1/2}(n)$ or $\epsilon_{2,5/2}(n)$ quantum defect for each level. Once the $\epsilon_{S_{1/2}}(n)$ and $\epsilon_{D_{5/2}}(n)$ are determined, the one photon $nS_{1/2} \rightarrow nP$ and $nD_{5/2} \rightarrow (n-3)F$ transitions yield in turn the $\epsilon_P(n)$ and $\epsilon_F(n)$ quantum defects, respectively. Figures 5–8 show in solid lines the variation of the quantum defects obtained in this way for the $S_{1/2}$, $D_{3/2,5/2}$, $P_{1/2,3/2}$, and $F_{5/2,7/2}$ levels. For the S and D quantum defects, we also show as a dashed line the variations of the "average quantum

TABLE I. Transition frequencies measured in this work. First and second columns give the quantum numbers of the initial and final state of each transition, the third column the observed frequency intervals with their estimated uncertainty. The last column gives the difference between the observed values and the ones predicted by formula (1) with the quantum defects calculated from Eq. (2) and Table IV. All figures are in MHz.

	Initial state n, l, J	Final state n', l', J'	Observed frequency interval ν' (MHz)	Observed calculated $\nu'-\nu$ (MHz)
$nS_{1/2}\rightarrow(n+1)S_{1/2}$	27, 0, $\frac{1}{2}$	28, 0, $\frac{1}{2}$	510 708.95 ± 0.2	−0.25
Two-photon	32 0, $\frac{1}{2}$	33 0, $\frac{1}{2}$	285 901.94 ± 0.2	0.02
transitions	33 0, $\frac{1}{2}$	34 0, $\frac{1}{2}$	257 744.27 ± 0.2	0.11
	34 0, $\frac{1}{2}$	35 0, $\frac{1}{2}$	233 166.19 ± 0.2	−0.04
	35 0, $\frac{1}{2}$	36 0, $\frac{1}{2}$	211 616.43 ± 0.2	−0.34
	36 0, $\frac{1}{2}$	37 0, $\frac{1}{2}$	192 643.05 ± 0.2	−0.25
	37 0, $\frac{1}{2}$	38 0, $\frac{1}{2}$	175 872.09 ± 0.2	−0.01
	38 0, $\frac{1}{2}$	39 0, $\frac{1}{2}$	160 992.71 ± 0.2	0.05
	39 0, $\frac{1}{2}$	40 0, $\frac{1}{2}$	147 745.64 ± 0.2	0.05
	40 0, $\frac{1}{2}$	41 0, $\frac{1}{2}$	135 912.97 ± 0.2	−0.03
	42 0, $\frac{1}{2}$	43 0, $\frac{1}{2}$	115 783.74 ± 0.2	−0.01
	44 0, $\frac{1}{2}$	45 0, $\frac{1}{2}$	99 441.22 ± 0.2	−0.06
$nS_{1/2}\rightarrow nP_{1/2}$	23, 0, $\frac{1}{2}$	23, 1, $\frac{1}{2}$	426 805.2 ± 2	0.74
Single-photon	25 0, $\frac{1}{2}$	25 1, $\frac{1}{2}$	316 960.8 ± 1	−0.07
transitions	26 0, $\frac{1}{2}$	26 1, $\frac{1}{2}$	275 996.57 ± 1	0.43
	27 0, $\frac{1}{2}$	27 1, $\frac{1}{2}$	241 797.50 ± 1	0.31
	28 0, $\frac{1}{2}$	28 1, $\frac{1}{2}$	213 022.07 ± 1	−0.83
	31 0, $\frac{1}{2}$	31 1, $\frac{1}{2}$	149 983.81 ± 2	−4.15
	32 0, $\frac{1}{2}$	32 1, $\frac{1}{2}$	134 578.00 ± 3	−3.25
	34 0, $\frac{1}{2}$	34 1, $\frac{1}{2}$	109 554.84 ± 4	−5.85
	39 0, $\frac{1}{2}$	39 1, $\frac{1}{2}$	69 170.10 ± 6	−2.57
	42 0, $\frac{1}{2}$	42 1, $\frac{1}{2}$	54 100.75 ± 10	−14.37
$nS_{1/2}\rightarrow nP_{3/2}$	23, 0, $\frac{1}{2}$	23, 1, $\frac{3}{2}$	455 977.40 ± 2	−2.43
Single-photon	25 0, $\frac{1}{2}$	25 1, $\frac{3}{2}$	338 704.70 ± 1	0.65
transitions	26 0, $\frac{1}{2}$	26 1, $\frac{3}{2}$	294 959.70 ± 1	1.59
	27 0, $\frac{1}{2}$	27 1, $\frac{3}{2}$	258 434.10 ± 1	1.33
	28 0, $\frac{1}{2}$	28 1, $\frac{3}{2}$	227 697.40 ± 1	−0.23
	30 0, $\frac{1}{2}$	30 1, $\frac{3}{2}$	179 426.20 ± 2	−1.22
	32 0, $\frac{1}{2}$	32 1, $\frac{3}{2}$	143 889.80 ± 3	−1.78
	34 0, $\frac{1}{2}$	34 1, $\frac{3}{2}$	117 148.90 ± 4	−4.08
	35 0, $\frac{1}{2}$	35 1, $\frac{3}{2}$	106 235.60 ± 5	−8.92

TABLE I. (*Continued.*)

	Initial state n, l, J	Final state n', l', J'	Observed frequency interval ν' (MHz)	Observed calculated $\nu'-\nu$ (MHz)
	38 0, $\frac{1}{2}$	38 1, $\frac{3}{2}$	80 663.80 ± 5	−0.59
	39 0, $\frac{1}{2}$	39 1, $\frac{3}{2}$	73 981.30 ± 6	−1.23
	40 0, $\frac{1}{2}$	40 1, $\frac{3}{2}$	68 016.00 ± 7	−2.74
	42 0, $\frac{1}{2}$	42 1, $\frac{3}{2}$	57 876.40 ± 8	−7.67
	44 0, $\frac{1}{2}$	44 1, $\frac{3}{2}$	49 655.00 ± 9	−11.80
$nD_{5/2}\rightarrow(n+1)D_{5/2,3/2}$	30, 2, $\frac{5}{2}$	31, 2, $\frac{5}{2}$	298 841.34 ± 0.2	−0.05
Two-photon	31 2, $\frac{5}{2}$	32 2, $\frac{5}{2}$	269 002.16 ± 0.2	0.09
transitions	31 2, $\frac{5}{2}$	32 2, $\frac{3}{2}$	266 666.04 ± 0.25	0
	35 2, $\frac{5}{2}$	36 2, $\frac{5}{2}$	182 612.71 ± 0.16	−0.03
	37 2, $\frac{5}{2}$	38 2, $\frac{5}{2}$	153 081.35 ± 0.14	0.03
$nD_{5/2}\rightarrow(n+2)P_{3/2}$	30, 2, $\frac{5}{2}$	32, 1, $\frac{3}{2}$	272 308.87 ± 3	1.80
Single-photon	37 2, $\frac{5}{2}$	39 1, $\frac{3}{2}$	139 360.00 ± 20	−15.48
transitions				
$nD_{5/2}\rightarrow(n-3)F_{7/2,5/2}$	27, 2, $\frac{5}{2}$	24, 3, $\frac{7}{2}$	261 619.10 ± 2	1.18
Single-photon	27 2, $\frac{5}{2}$	24 3, $\frac{5}{2}$	261 549.60 ± 1.5	0.98
transitions	28 2, $\frac{5}{2}$	25 3, $\frac{7}{2}$	231 758.80 ± 1.6	−0.34
	29 2, $\frac{5}{2}$	26 3, $\frac{7}{2}$	206 275.50 ± 1.5	−0.79
	30 2, $\frac{5}{2}$	27 3, $\frac{7}{2}$	184 396.00 ± 1.7	−0.28
	32 2, $\frac{5}{2}$	29 3, $\frac{7}{2}$	149 110.20 ± 2	3.02
	32 2, $\frac{5}{2}$	29 3, $\frac{5}{2}$	149 069.30 ± 1	1.37
	33 2, $\frac{5}{2}$	30 3, $\frac{7}{2}$	134 810.80 ± 4	4.41
	33 2, $\frac{5}{2}$	30 3, $\frac{5}{2}$	134 774.20 ± 4	3.26
	36 2, $\frac{5}{2}$	33 3, $\frac{7}{2}$	101 537.00 ± 20	20.30

defects" $\epsilon^*(n)$ used as an intermediate step for the quantum-defect calculation. With our experiments, only one point was available for the $\epsilon_{2,3/2}$ quantum defects (from $31D_{5/2}\rightarrow 32D_{3/2}$ transition). In order to obtain the slope $a_{2,3/2}$, we have calculated the binding energies of the $nD_{3/2}$ levels by adding the nD fine-structure intervals measured in Ref. 6 to the $nD_{5/2}$ binding energies obtained from the knowledge of the $\epsilon_{2,5/2}(n)$ quantum-defect values. This procedure gives us the triangles in Fig. 6, which fall on a straight line connected to our own measured point. The values of the $\epsilon_{lJ}(\infty)$ and a_{lJ} coefficients deduced from these measurements are gathered in Table IV. Note that the slopes of the quantum defects $\epsilon_{lJ}(n)$ versus $1/n^{*2}$ are positive for the S, P, and D states (penetrating orbitals) and negative for F states (nonpenetrating ones).

It is interesting to compare these values with the best results obtained by optical methods by Lorenzen *et al.*[6,7] (dotted lines in Figs. 5–8 and values

TABLE II. Experimental values of fine-structure intervals in Cs. Very excited state structures ($n \geq 23$) are obtained by microwave spectroscopy (this work). The more bound-state structures ($n \leq 17$) are obtained from optical experiments (references in the table). The last column gives the difference between the measured values and the ones predicted by expressions (6) and (7) with the coefficients given in Table V. Note the change in frequency units inside the table.

	Initial state			Final state			Fine-structure measured interval	Observed − Calculated
	n,	l,	J	n,	l,	J'		
$\Delta(nP_{1/2}\rightarrow nP_{3/2})$	7,	1,	$\frac{1}{2}$	7,	1,	$\frac{3}{2}$	5428.19 ± 1.8 (GHz)	0.39 (GHz)
Optical	8	1,	$\frac{1}{2}$	8	1,	$\frac{3}{2}$	2479.13 ± 1.8	−0.90
experiment	9	1,	$\frac{1}{2}$	9	1,	$\frac{3}{2}$	1338.57 ± 1.8	−1.76
(Ref. 7)	10	1,	$\frac{1}{2}$	10	1,	$\frac{3}{2}$	805.84 ± 1.8	0.02
	11	1,	$\frac{1}{2}$	11	1,	$\frac{3}{2}$	522.54 ± 1.8	0.62
	12	1,	$\frac{1}{2}$	12	1,	$\frac{3}{2}$	356.60 ± 1.8	0.64
	13	1,	$\frac{1}{2}$	13	1,	$\frac{3}{2}$	254.82 ± 1.8	−0.37
$\Delta(nP_{1/2}\rightarrow nP_{3/2})$	23,	1,	$\frac{1}{2}$	23,	1,	$\frac{3}{2}$	29172.20 ± 4 (MHz)	−0.02 (MHz)
This work	25	1,	$\frac{1}{2}$	25	1,	$\frac{3}{2}$	21744.00 ± 1	0.82
(microwave	26	1,	$\frac{1}{2}$	26	1,	$\frac{3}{2}$	18963.20 ± 1	0.42
experiment)	27	1,	$\frac{1}{2}$	27	1,	$\frac{3}{2}$	16636.65 ± 1	−0.27
	28	1,	$\frac{1}{2}$	28	1,	$\frac{3}{2}$	14676.00 ± 1	−0.39
	32	1,	$\frac{1}{2}$	32	1,	$\frac{3}{2}$	9310.35 ± 1	−1.93
	34	1,	$\frac{1}{2}$	34	1,	$\frac{3}{2}$	7593.00 ± 1	−1.13
	39	1,	$\frac{1}{2}$	39	1,	$\frac{3}{2}$	4811.20 ± 2	−0.12
	42	1,	$\frac{1}{2}$	42	1,	$\frac{3}{2}$	3775.60 ± 10	5.42
$\Delta(nF_{7/2}\rightarrow nF_{5/2})$	10,	3,	$\frac{7}{2}$	10,	3,	$\frac{5}{2}$	873.20 ± 2 (MHz)	4.97 (MHz)
Laser	11	3,	$\frac{7}{2}$	11	3,	$\frac{5}{2}$	667.20 ± 2	−0.01
experiment	12	3,	$\frac{7}{2}$	12	3,	$\frac{5}{2}$	522.00 ± 3	−0.66
(Ref. 5)	13	3,	$\frac{7}{2}$	13	3,	$\frac{5}{2}$	416.00 ± 3	−0.45
	14	3,	$\frac{7}{2}$	14	3,	$\frac{5}{2}$	336.80 ± 1	−0.03
	15	3,	$\frac{7}{2}$	15	3,	$\frac{5}{2}$	276.30 ± 1	0.21
	16	3,	$\frac{7}{2}$	16	3,	$\frac{5}{2}$	229.30 ± 1	0.31
	17	3,	$\frac{7}{2}$	17	3,	$\frac{5}{2}$	190.50 ± 2	−1.45
$\Delta(nF_{7/2}\rightarrow nF_{5/2})$	24,	3,	$\frac{7}{2}$	24,	3,	$\frac{5}{2}$	69.58 ± 2 (MHz)	−0.04 (MHz)
This work	29	3,	$\frac{7}{2}$	29	3,	$\frac{5}{2}$	40.32 ± 3	0.61
	30	3,	$\frac{7}{2}$	30	3,	$\frac{5}{2}$	36.60 ± 4	0.70
$\Delta(nD_{3/2}\rightarrow nD_{5/2})$	32,	2,	$\frac{3}{2}$	32,	2,	$\frac{5}{2}$	2336.13 ± 0.2 (MHz)	0.01 (MHz)
This work								

TABLE III. Hyperfine-structure intervals in the $nS_{1/2}$ and $nP_{1/2}$ levels of cesium measured in this work (in MHz).

n	$nS_{1/2}$ $(F=3\rightarrow F=4)$	$nP_{1/2}$ $(F=3\rightarrow F=4)$
23	9.2±0.8	2.23±0.2
25	5.8±0.8	1.60±0.2
26	5.7±0.8	1.25±0.2
28	4.7±0.8	1.10±0.2

in parentheses in Table IV). Our data for the $\epsilon_{lJ}(\infty)$ are one order of magnitude more precise, with a fair agreement within the quoted uncertainties of Ref. 7 for the nP levels, and a very slight discrepancy for the nS and nD levels.[6] The a_{lJ} coefficients are in good agreement. (Note that for the case of D states, the quantum defects are constant within the limits of uncertainty in the optical measurements.[6])

It is worth noticing that our quantum-defect analysis does not depend on the value of the ionization energy E_i of cesium. We can thus use our ϵ's to determine the binding energies of the nS and nD states and, by adding these energies to the transition energies to the ground state measured in Ref. 6, we obtain a new measure of E_i. Analyzing in such a way 13 nS levels and 21 $nD_{5/2}$ levels with $n > 20$, we find as a mean value

$$E_i = 31\,406.4676(33)\ \text{cm}^{-1}\ ,$$

the quoted error being the standard deviation of all results. This value agrees remarkably well with the one given in Ref. 6 [31 406.468(6) cm^{-1}] and has a slightly smaller uncertainty.

The precision of our quantum-defect fit for the transition frequencies is attested by the last column of Table I which gives in MHz the difference between the measured frequency and the one predicted by formulas (1) and (2) with the $\epsilon_{lJ}(\infty)$ and a_{lJ} given by Table IV. All two-photon transition frequencies are predicted with a few tens of kHz uncertainty, whereas most single-photon transitions are calculated with a $\sim$1-MHz accuracy. The discrepancies are larger only for some transitions involving very excited states with $n > 32$, where Stark shifts due to stray electric fields and resonance broadenings due to microwave saturation are

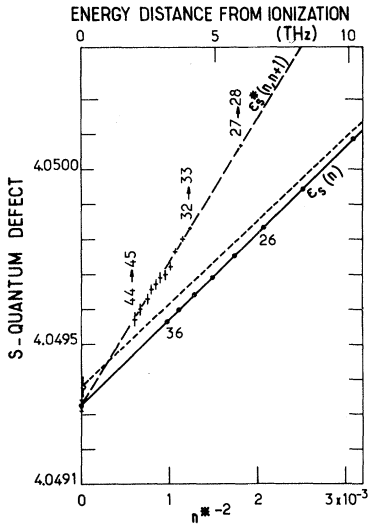

FIG. 5. nS quantum defect $\epsilon_{0,1/2}(n)$ plotted against the inverse squared effective quantum number $n^{*-2}\simeq(n-4.0493)^{-2}$. Dashed line gives, as an intermediate step, the variation of the average quantum defect $\epsilon^*_S(n,n+1)$ evaluated from each $nS\rightarrow(n+1)S$ transition frequency. Solid line gives the actual quantum-defect variation. Crosses correspond to the measured frequencies (with their error bars). Dotted line is the result of Lorenzen *et al.* (Ref. 6) and the error bar on this dotted line gives an estimate of their uncertainties.

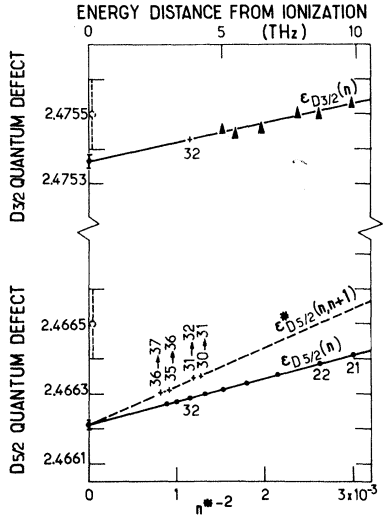

FIG. 6. Plot of the D quantum defects vs $n^{*-2}\simeq(n-2.471)^{-2}$. In order to obtain the $\epsilon_{D_{5/2}}(n)$ variation, one has first determined the average quantum number $\epsilon^*_{D5/2}(n)$, obtained from the $nD_{5/2}\rightarrow(n+1)D_{5/2}$ transition frequencies. (Dashed line: same procedure as for the nS quantum defects.) $\epsilon_{D_{3/2}}(n)$ law is extrapolated from the $31D_{5/2}\rightarrow32D_{3/2}$ transition (cross) and the fine-structure measurements of Ref. 6 (triangles). $\epsilon(\infty)$ values of Lorenzen *et al.* (Ref. 6) are given with their error bars.

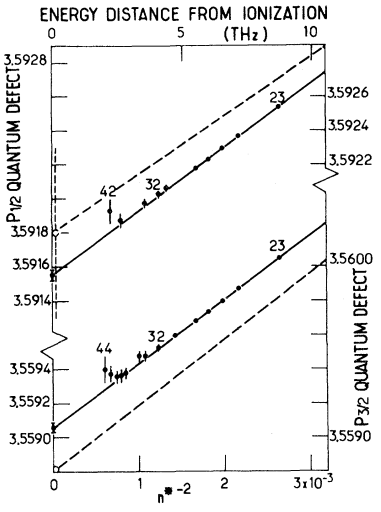

FIG. 7. $nP_{1/2}$ and $nP_{3/2}$ quantum defects $\epsilon_{1,1/2}(n)$ and $\epsilon_{1,3/2}(n)$ plotted against $n^{*-2}\simeq(n-3.5757)^{-2}$. Dots (with error bars) correspond to the values deduced from measured frequencies. Linear variation laws (solid lines) have been obtained by a least-squares fit limited to the less excited $23\leq n\leq 32$ levels. Systematic deviations observed for $n>32$ are attributed to stray field induced Stark effects. Dotted lines are the Lorenzen and Niemax (Ref. 7) results. Note the large error bar on the position of these lines.

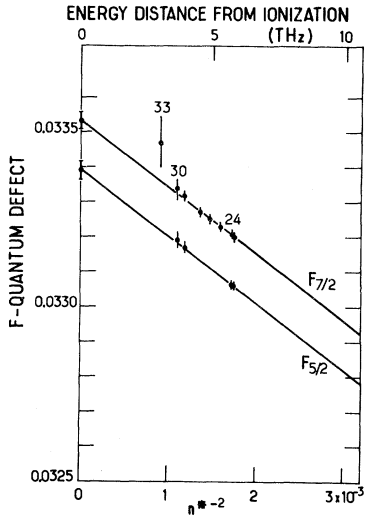

FIG. 8. nF quantum defects $\epsilon_{3,5/2}(n)$ and $\epsilon_{3,7/2}(n)$ plotted against $n^{*-2}\simeq(n-0.033)^{-2}$. Parallel solid lines indicate that the fine structure remains certainly inverted up to the ionization limit.

likely to perturb the extremely polarizable levels. The two-photon S-S and D-D measured frequencies fit much better the predictions even for high n's because the two levels involved in the transition are

TABLE IV. The $\epsilon_{l,J}(\infty)$ and $a_{l,J}$ coefficients of the cesium quantum defects measured in this work with their uncertainties. Best optical values, obtained by Lorenzen *et al.* (Refs. 6 and 7), are given in parentheses for comparison.

	$\epsilon_{l,J}(\infty)$	$a_{l,J}$
$nS_{1/2}$	$4.049\,325\pm1.5\times10^{-5}$ $(4.049\,38\pm3\times10^{-5})$	$0.246\,2\pm5\times10^{-3}$ $(0.236\,5\pm1.9\times10^{-3})$
$nP_{1/2}$	$3.591\,556\pm3\times10^{-5}$ $(3.591\,8\pm5\times10^{-4})$	$0.371\,4\pm4\times10^{-3}$ $(0.342\pm9\times10^{-3})$
$nP_{3/2}$	$3.559\,058\pm3\times10^{-5}$ $(3.558\,8\pm1\times10^{-3})$	$0.374\pm4\times10^{-3}$ $(0.386\pm1\times10^{-3})$
$nD_{3/2}$	$2.475\,365\pm2\times10^{-5}$ $(2.475\,5\pm1\times10^{-4})$	$0.555\,4\pm6\times10^{-3}$ $(-0.003\pm2.4\times10^{-2})$
$nD_{5/2}$	$2.466\,210\pm1.5\times10^{-5}$ $(2.466\,5\pm1\times10^{-4})$	$0.067\pm5\times10^{-3}$ $(-0.030\pm2.7\times10^{-2})$
$nF_{5/2}$	$0.033\,392\pm3\times10^{-5}$	$-0.191\pm3\times10^{-2}$
$nF_{7/2}$	$0.033\,537\pm2.5\times10^{-5}$	$-0.191\pm2\times10^{-2}$

in this case similar and experience almost the same Stark shift, which cancels out in the measured frequency. This cancellation does not occur in the $S \rightarrow P$ and $D \rightarrow F$ one-photon transitions linking unlike states with different polarizabilities.

IV. ANALYSIS OF THE DATA: FINE STRUCTURES

The J dependence of the quantum defects expresses the fact that the fine-structure intervals in Rydberg levels can be developed as an expansion in powers of $n^* = n - \epsilon(n)$ of the form

$$\Delta_{fs} = An^{*-3} + Bn^{*-5} + Cn^{*-7} + \cdots . \quad (3)$$

Our fine-structure data can be summarized in the following expressions, where only the leading n^{*-3} term has been retained:

$$\Delta_{fs}(nP) = 2.1383(2) \times 10^8 (n - 3.5757)^{-3} \text{ MHz} , \quad (4)$$

with 3.5757 being the average quantum defect of the $P_{1/2}$ and $P_{3/2}$ levels in the range $23 \leq n \leq 42$;

$$\Delta_{fs}(nF) = -9.7(2) \times 10^5 (n - 0.033\,15)^{-3} \text{ MHz} , \quad (5)$$

where 0.033 15 is the average quantum defect of the $nF_{5/2}$ and $nF_{7/2}$ levels around $n = 30$. Extrapolation of these simple formulas to lower n values give results in fair agreement with the determination of these quantities in more tightly bound states. However, in order to get an excellent fit over the whole n range, one has to take into account higher-order terms in expression (3), and $\epsilon(n)$ variations in the determination of n^*.

For all fine structures we propose the following formula, valid even for low excited states:

$$\Delta_{fs}(n,l,J \rightarrow n,l,J+1) = A[n - \epsilon_{l,J,J+1}(n)]^{-3} + B[n - \epsilon_{l,J,J+1}(n)]^{-5} + C[n - \epsilon_{l,J,J+1}(n)]^{-7} , \quad (6)$$

where the average quantum defect $\epsilon_{l,J,J+1}(n)$ is

$$\epsilon_{l,J,J+1}(n) = \tfrac{1}{2}[\epsilon_{l,J}(n) + \epsilon_{l,J+1}(n)] = \epsilon_{l,J,J+1}(\infty) + a_{l,J,J+1}[n - \epsilon_{l,J,J+1}(\infty)]^{-2} . \quad (7)$$

The values of the parameters A, B, C, $\epsilon_{l,J,J+1}(\infty)$, and $a_{l,J,J+1}$ are given in Table V.

The last column in Table II gives the difference between the observed fine-structure intervals and the values calculated from Eqs. (6) and (7) with the values of the parameters in Table V. The agreement is excellent over a large domain of n values for nP as well as for nF fine-structure intervals (the typical relative discrepancy is smaller than 0.1%).

For the nD fine structures, in spite of the fact that we have measured only one interval, it is nevertheless possible to develop a similar procedure: our very precise measure gives with a great accuracy the An^{*-3} term. The deviation with respect to the n^{*-3} law of the intervals measured by optical methods for the more tightly bound levels[6] obeys an n^{*-5} law, for which we obtain the B coefficient given in Table V (the n^{*-7} contribution is not noticeable for the optical series with $n \geq 11$). The agreement of the observed nD interval with our variation law $An^{*-3} + Bn^{*-5}$ is still excellent (accuracy better than 1%).

TABLE V. Coefficients for fine-structure intervals in cesium according to eqs. (6) and (7).

	$A_{(\text{MHz})}$	$B_{(\text{MHz})}$	$C_{(\text{MHz})}$	$\epsilon_{l,J,J+1}(\infty)$	$a_{l,J,J+1}$
$nP_{1/2} \rightarrow nP_{3/2}$	$2.139\,25(20) \times 10^8$	$-5.6(4) \times 10^7$	$3.9(1) \times 10^8$	3.575 31	0.3727
$nD_{3/2} \rightarrow nD_{5/2}$	$6.021\,83(60) \times 10^7$	$-5.8(8) \times 10^7$	0	2.470 79	0.0612
$nF_{5/2} \rightarrow nF_{7/2}$	-9.796×10^5[a]	1.222×10^7[a]	-3.376×10^7[a]	0.033 46	−0.191

[a]The values for the nF fine structure are coming from Ref. 5. The others are from our determination taking into account our present microwave experiment, together with the optical results (6) and (7).

ACKNOWLEDGMENTS

Thanks are due to Dr. R. Adde (Electronique Fondamentale, Orsay) and to Dr. A. Clairon (L.P.T.F., Observatoire de Paris) for the lending of equipment. One of the authors (P.G.) would like to express his gratitude to A. Clairon for many fruitful discussions.

[1]C. Fabre, S. Haroche, and P. Goy, Phys. Rev. A 18, 229 (1978).
[2]P. Goy, C. Fabre, M. Gross, and S. Haroche, J. Phys. B 13, L83 (1980).
[3]C. Fabre, S. Haroche, and P. Goy, Phys. Rev. A 22, 778 (1980).
[4]P. Goy, Int. J. Infrared Millimeter Waves (1982).
[5]K. Fredriksson, H. Lundberg, and S. Svanberg, Phys. Rev. A 21, 241 (1980).
[6]C. J. Lorenzen, K. H. Weber, and K. Niemax, Opt. Commun. 33, 271 (1980).
[7]C. J. Lorenzen and K. Niemax, J. Quant. Spectrosc. Radiat. Transfer 22, 247 (1979).